Simulation of nearly missing helicopters through the computational fluid dynamics approach

Momoha Nishimura[1[0000-0002-7727-4566]] and Masashi Yamakawa[1[0000-0001-5960-2602]]

[1] Kyoto Institute of Technology, Matsugasaki, Sakyo, 606-8585 Kyoto, Japan
d7821007@edu.kit.ac.jp

Abstract. This study achieves modelling two helicopters via computational fluid dynamics (CFD) and simulating the flow field that develops due to a near miss. The rotation of the main rotor and the translational movement of the helicopter are modelled in this study, and the long trajectory of the moving helicopter is realised in the simulation. Moreover, the interaction of flows around the two moving helicopters is also achieved by introducing the communication between multiple moving computational domains. Firstly, the validation test is conducted using a helicopter model with a rotating main rotor, where the results produced by our in-house code are compared with those computed by another CFD solver, *FaSTAR-Move*. This test verifies that the communication between the overlapping grids is reliably achieved in our simulation. In the simulation of nearly missing helicopters, two near-miss cases are computationally demonstrated, where the complex flow field which develops around the two helicopters is captured, and the disturbance in aerodynamic and moment coefficients exerted on the helicopters are observed. These results confirm the capability of this CFD approach for realising near-miss events on a computer.

Keywords: CFD, moving grids, overset methods, helicopter.

1 Introduction

Recently, the airspace in metropolitan areas has become extremely busy: there are commercial helicopters, police helicopters, and medevac flights, and the demand for air transport by aeroplanes has been increasing greatly. Moreover, considering the current expansion of drone industries and the launch of flying cars in the future, aircraft will need to share more congested airspace. While the danger of crashing need hardly be said, there is also the risk of near-miss flights, where aircraft are affected by the flow field that develops around other aircraft. In fact, the near collision of two helicopters has been reported [1]. Considering the increasing congestion of the future airspace, near-miss events will occur more frequently. Therefore, comprehending the aerodynamic effects exerted on aircraft and their behaviour in response to the effects in a near miss is essential to ensure the safety of aircraft as well as promoting legislation to introduce standards that increase the safety of aircraft in more congested airspace. However, since the flight in this scenario involves high risk, flight tests by real aircraft are not easily manageable. On the other hand, computational fluid dynamics (CFD) allows

ICCS Camera Ready Version 2022
To cite this paper please use the final published version:
DOI: 10.1007/978-3-031-08760-8_28

an arbitrary scenario to be set and high-risk flight simulations to be conducted without risking human life. Thus, it is essential to further develop the CFD method to computationally examine the nearly missing aircraft.

The current CFD used for analysing the flow around aircraft is able to not only simulate fully fixed objects but also model their moving and deforming components and analyse the flow field in detail. For example, CFD simulations for helicopters analysed the flow generated by their rotors and its aerodynamic effects in combination with wind tunnel testing [2, 3]. The trajectory prediction of aircraft through CFD has also been reported [4]. The manoeuvring of aircraft has been simulated through the coupled simulation of CFD and flight dynamics that considers the configuration of the components, their function, and the controlling system. This approach is effective for analysing the flow field and the reaction of aircrafts to the flow field [5]. However, these simulations have primarily been used to model only one aircraft, and near-miss events involve multiple aircraft. This implies that the CFD method, which can model multiple moving objects and the interaction of the flow fields generated by them, is necessary for simulating near-miss events on a computer.

Therefore, in this paper, we simulate two helicopters in a near miss using the CFD method. Helicopters are chosen as models for the first application of the CFD approach for near-miss events based on an actual reported occurrence of a near miss involving helicopters [1]. The rotation of the main rotor and the translational movement of the helicopters are realised in the simulation, and the two helicopter models are crossed in a remarkably close context. The translation is simulated by a moving mesh method, in particular the moving-grid finite volume (MGFV) method [6]. This satisfies the geometric conservation law (GCL) condition by employing a unified space-time, four-dimensional control volume for the discretisation. The moving computational domain (MCD) method [7] is applied to modelling the helicopters that travel over long trajectories, which allows the complex flow field around moving helicopters to be realised instead of modelling fixed objects in the context of wind tunnel testing. The MCD method removes the spatial limitation for simulating objects with long trajectories that occurs due to computational cost. In this method, a large background mesh is not required, and thus objects can move freely in a three-dimensional space because the computational domains are moved in line with the motions of an object inside [8, 9]. Conventionally, it was difficult for the MCD method to gain information from outside the computational domain created for the enclosed object, and therefore the simulation was targeted at only one object. However, introducing the overset approach to the MCD method allowed communication between the domains created around each moving object [10]. In this study, the flow field variables are communicated between the main rotor grid and the fuselage grid of the helicopter, which model the rotation of the main rotor. There is also communication between the flow fields around the two moving helicopters to represent the flow interaction around them. Using these methods realised the near-miss flight simulation of helicopters and calculated the aerodynamic forces exerted on each helicopter during the near miss.

ICCS Camera Ready Version 2022
To cite this paper please use the final published version:
DOI: 10.1007/978-3-031-08760-8_28

2 Numerical methods

2.1 CFD solver

The three-dimensional Euler equations for compressible flow are adopted as a governing equation:

$$\frac{\partial \boldsymbol{q}}{\partial t} + \frac{\partial \boldsymbol{E}}{\partial x} + \frac{\partial \boldsymbol{F}}{\partial y} + \frac{\partial \boldsymbol{G}}{\partial z} = \mathbf{0}, \tag{1}$$

where $\boldsymbol{q}$ represents a vector of conserved variables, and $\boldsymbol{E}$, $\boldsymbol{F}$, and $\boldsymbol{G}$ denote the inviscid flux vectors. t indicates time, and x, y, z are the coordinates. This system is closed by assuming the ideal gas law, where the ratio of specific heats $\gamma = 1.4$ is used.

Equation (1) is discretised by the cell-centred MGFV method, which uses a unified space-time, four-dimensional control volume for the discretisation [6, 10], yielding the following formulae with the variables in the current N step and the next $N+1$ step:

$$\begin{gathered}\boldsymbol{q}^{N+1}(\tilde{n}_t)_6 + \boldsymbol{q}^{N}(\tilde{n}_t)_5 + \sum_{l=1}^{4}\left\{\boldsymbol{q}^{N+\frac{1}{2}}\,\tilde{n}_t + \boldsymbol{H}^{N+\frac{1}{2}}\right\}_l = 0 \\ \boldsymbol{H} = \boldsymbol{E}\tilde{n}_x + \boldsymbol{F}\tilde{n}_y + \boldsymbol{G}\tilde{n}_z \\ \boldsymbol{q}^{N+\frac{1}{2}} = \frac{1}{2}(\boldsymbol{q}^{N} + \boldsymbol{q}^{N+1}), \qquad \boldsymbol{H}^{N+\frac{1}{2}} = \frac{1}{2}(\boldsymbol{H}^{N} + \boldsymbol{H}^{N+1}),\end{gathered} \tag{2}$$

where $\tilde{\boldsymbol{n}} = [\tilde{n}_t, \tilde{n}_x, \tilde{n}_y, \tilde{n}_z]$ represents the four-dimensional outward normal vector of the control volume. Roe's flux difference splitting (FDS) [11] is used to estimate the inviscid flux vector $\boldsymbol{H}_l$, and the MUSCL (monotonic upstream-centred scheme for conservation laws) scheme is applied to provide second-order accuracy. The primitive variables of $\boldsymbol{q}$ are reconstructed by the gradient, which is evaluated by the least-squares approach and Hishida's limiter [12]. $(\boldsymbol{q}\tilde{n}_t)_l$ in Eq. (2) is estimated by the following upwind scheme:

$$(\boldsymbol{q}\tilde{n}_t)_l = \frac{1}{2}[\boldsymbol{q}^{+}\tilde{n}_t + \boldsymbol{q}^{-}\tilde{n}_t - |\tilde{n}_t|(\boldsymbol{q}^{+} - \boldsymbol{q}^{-})].$$

Unsteady flow is solved by a pseudo-time approach with the two-stage rational Runge-Kutta (RRK) scheme for the pseudo-time stepping.

2.2 MCD method

The movement of objects with long trajectories is expressed by the MCD method [7]. Computational domains created around each object move in line with the motions of the object inside, and therefore this approach makes it possible for objects to move freely without any spatial limitations. However, because it is difficult for objects to

ICCS Camera Ready Version 2022
To cite this paper please use the final published version:
DOI: 10.1007/978-3-031-08760-8_28

obtain information from outside their computational domains, simulating the interaction of flow fields around multiple moving objects is challenging. Therefore, the overset approach described in the following section is introduced to allow communication between the computational domains (Fig. 1).

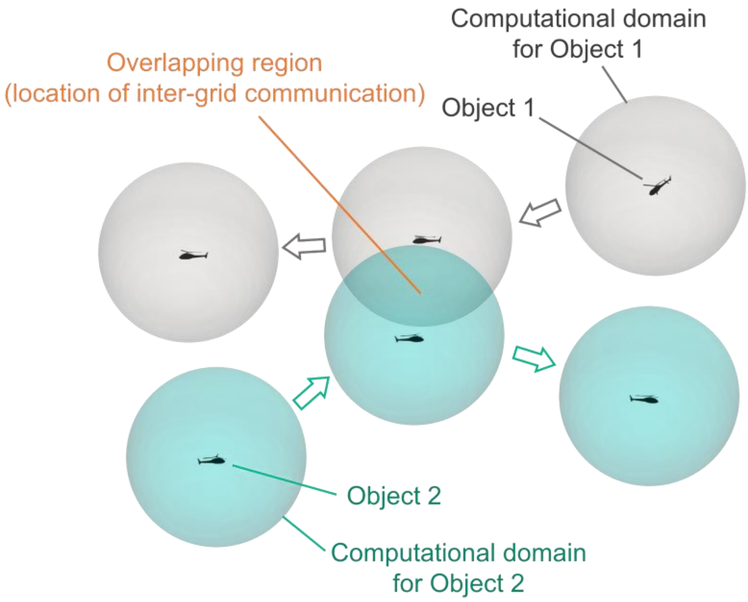

Fig. 1. The concept of the MCD method for multiple moving objects

2.3 Inter-grid communication for multiple moving computational domains

The variables of each computational domain communicate in their overlapping region by applying the overset approach. The implicit hole cutting (IHC) of the overset approach can be described by the following procedure. First, the cell in the overlapping partner grid that includes the nodes of the target grid is determined. Here the KD-tree-based algorithm is used to search for the owner cells. Then, nodes and cells are classified using the method proposed by Nakahashi [13]. In this method, the node type is designated by comparing the distances between the node and the object in the target grid and between the same position in the overlapping partner grid and the object. The nodes which have shorter distances are designated as active cells and those with longer distances are designated as nonactive cells. A tetrahedron cell which consists of all nonactive nodes is a nonactive cell, for which variables are not computed. The cells which overlap the object of the partner grid are also designated as nonactive cells. Conversely, a cell whose nodes are all active is an active cell. The remaining cells are interpolation cells, where the flow field variables are interpolated from the overlapping partner grid, based on the values of so-called donor cells in the partner grid. The donor cells surround the interpolation cells. Inverse distance weighing is employed as the interpolation method.

ICCS Camera Ready Version 2022
To cite this paper please use the final published version:
DOI: 10.1007/978-3-031-08760-8_28

3 Validation test

The in-house code was validated by comparing the results computed by an unstructured overset grid CFD solver *FaSTAR-Move* [14, 15], which was developed by Japan Aerospace Exploration Agency (JAXA). *FaSTAR-Move* is not suitable for simulating objects which travel over long trajectories although it can model the deformation and short movement of objects by using the overset method. Therefore, in this test, a helicopter model is placed in uniform flow instead of using the MCD method and moving the whole model in a three-dimensional space. The computational grids created around the fuselage are fixed, while the other grids created around the main rotor rotate. The fuselage grid and the main rotor grid communicate with each other using the overset approach. This validation aims to confirm that the overset approach in the in-house code accurately interpolates the variables between the overlapping grids.

3.1 Helicopter model

This study used a simplified helicopter model based on the AS-355 helicopter without the tail rotor. The origin of the body axes used for calculating the rolling, pitching, and yawing moment is the centre of mass, as illustrated in Fig. 2. The centre of mass was calculated from the polygons of the fuselage and the main rotor. The fuselage length of 11.2 m was normalised to 1 in the model.

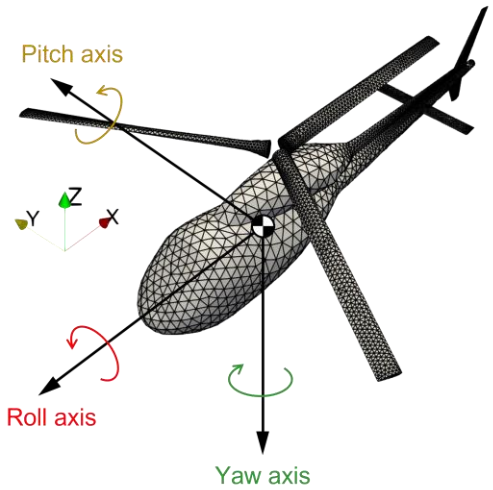

Fig. 2. Helicopter model

3.2 Computational conditions

A cubic computational domain with a side of $30L$ was created around the fuselage (Fig. 3a), where the fuselage length is L. Another computational domain was created around the main rotor (Fig. 3b). 407,079 cells for the fuselage and 151,927 cells for the main rotor were generated by an unstructured mesh generator *MEGG3D* [16].

ICCS Camera Ready Version 2022
To cite this paper please use the final published version:
DOI: 10.1007/978-3-031-08760-8_28

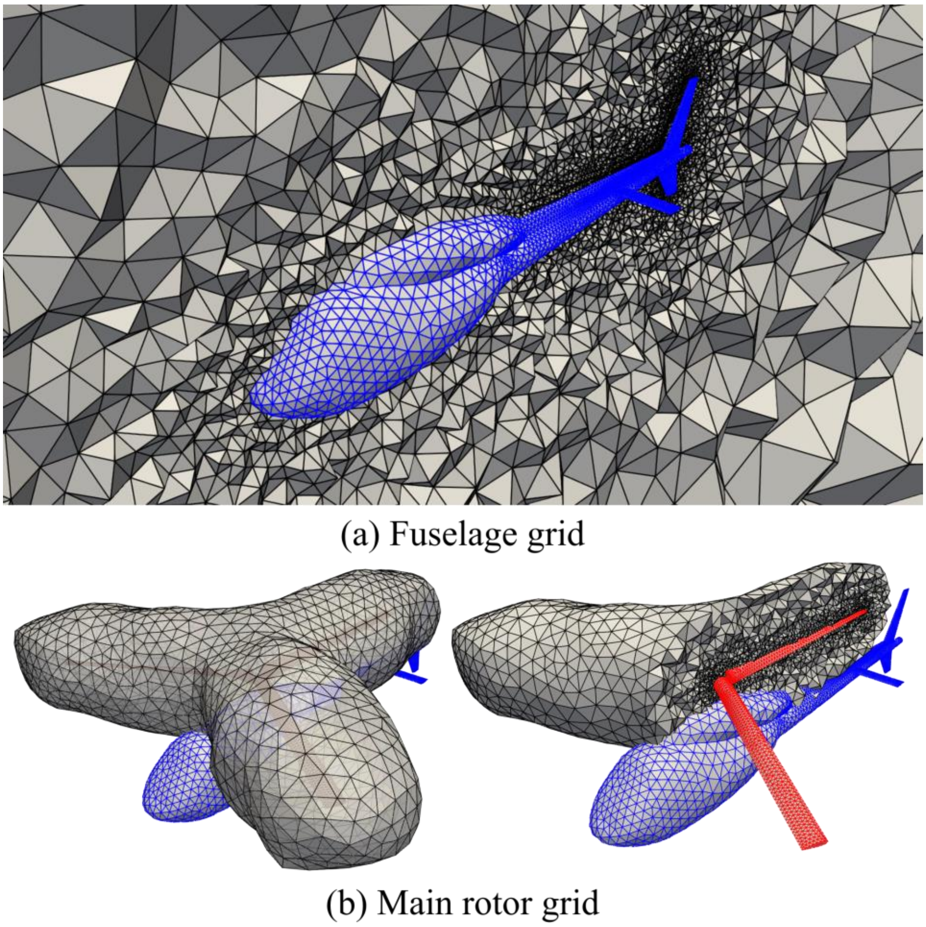

Fig. 3. Computational domains for (a) the fuselage and (b) main rotor

The velocity of the uniform flow is Mach 0.2 in the x direction, as the cruising speed of the helicopter is assumed to be approximately Mach 0.2. The main rotor and grids around it rotate counterclockwise at 395 rpm. In this study, the main rotor performs rotation only.

Table 1 shows the numerical method used in *FaSTAR-Move*. The numerical method of the in-house code is given in Table 1, and it is described in Section 2. The boundary conditions are the slip conditions at the surfaces of the fuselage and the main rotor, the uniform inflow conditions at the yz-plane of the outer boundary which the helicopter faces, and the Riemann invariant boundary conditions at the remaining outer boundaries of the fuselage grid. The variables are interpolated from the fuselage grid at the outer boundary of the main rotor grid unless the boundary cell is a nonactive cell.

ICCS Camera Ready Version 2022
To cite this paper please use the final published version:
DOI: 10.1007/978-3-031-08760-8_28

Table 1. Numerical methods used for the validation test

	FaSTAR-Move	**In-house code**
Governing equation	3-D compressible Euler	3-D compressible Euler
Advection term	SLAU [17]	Roe's FDS
Reconstruction	Weighted Green-Gauss	Least square
Slope limiter	Hishida (van Leer)	Hishida (van Leer)
Time integration	LU-SGS (Lower-upper symmetric Gauss-Seidel)	RRK
Interpolation	Tri-linear interpolation	Inverse distance weighted interpolation

3.3 Results and discussion

The graph in Fig. 4 depicts the time history of the pressure coefficient computed for the fuselage surface of the helicopter and compares it with the results provided by *FaSTAR-Move*. The position of the main rotor after it rotated for 1.0 s from the beginning of the calculation was set as 0 deg, and the figure shows the data while the main rotor rotates three complete rotations from the 0-deg position. Figure 4 indicates that the same trend can be seen in the pressure coefficient between the in-house code and *FaSTAR-Move*, although there is not exact agreement due to the differences of the numerical schemes and interpolation methods between the two software codes. Three peaks can be observed for one rotation, indicating that the pressure oscillation, which was raised by the flow generated by the three blades of the main rotor, was captured on the fuselage surface. The characteristics of the oscillation predicted in the present study, in particular the position and values of the coefficient peaks, are in line with the values predicted by *FaSTAR-Move*, instilling confidence that the flow field variables are accurately communicated between the overlapping grids in the in-house code.

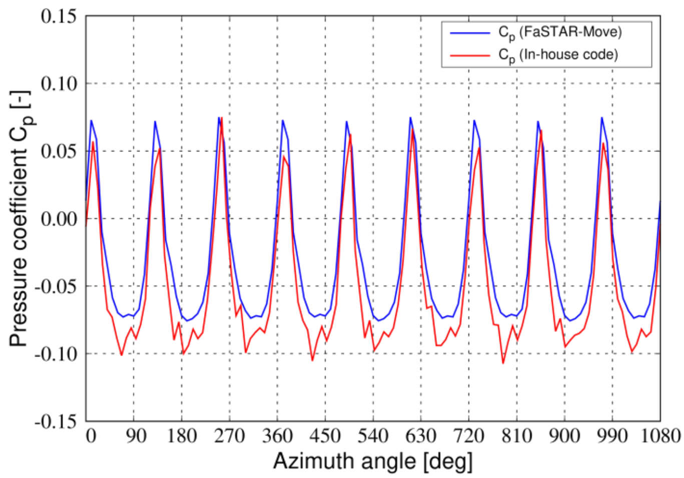

Fig. 4. Comparison of the pressure coefficients computed with *FaSTAR-Move* and the in-house code

ICCS Camera Ready Version 2022
To cite this paper please use the final published version:
DOI: 10.1007/978-3-031-08760-8_28

4 Simulation of nearly missing helicopters

4.1 Configurations of the test cases

Two cases were tested in which aerodynamic effects were assumed to be exerted on helicopters. Figure 5 shows the flight paths in the two cases. In Case 1, illustrated in Fig. 5a, the trajectories of the two helicopters intersect perpendicularly, where Helicopter 2 passes just behind the trajectory of Helicopter 1. Helicopter 2 flies slightly above Helicopter 1 to avoid colliding their blades. In Case 2, Helicopter 2 passes horizontally underneath Helicopter 1, where the trajectory of Helicopter 2 does not pass directly below that of Helicopter 1 but slightly shifted in the y direction, as depicted in Fig. 5b.

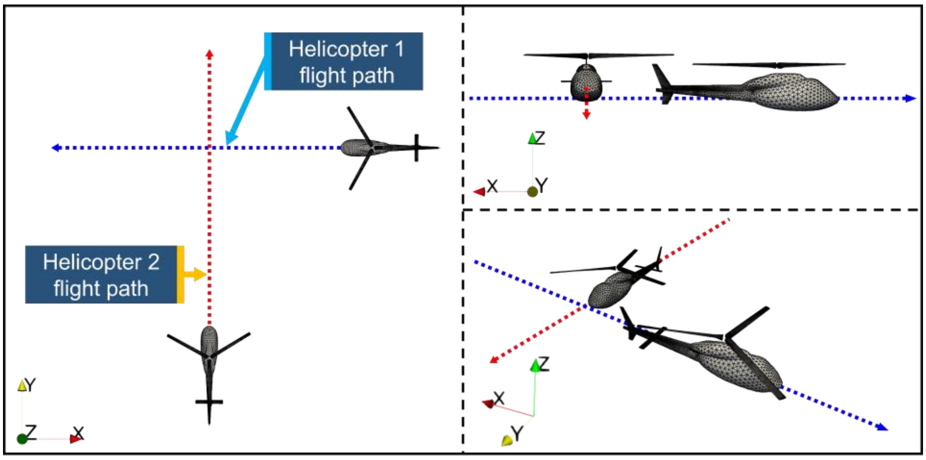

(a) Case 1

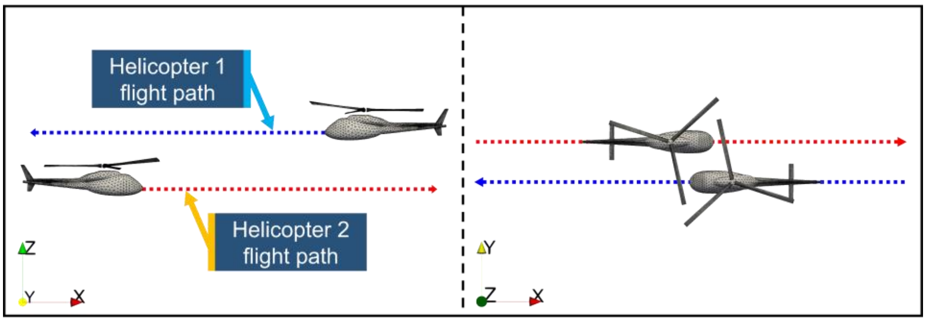

(b) Case 2

Fig. 5. Flight paths of the two test cases

ICCS Camera Ready Version 2022
To cite this paper please use the final published version:
DOI: 10.1007/978-3-031-08760-8_28

4.2 Computational conditions

The helicopter model described in Section 3.1 was used for the test cases of nearly missing helicopters. A spherical computational domain with a diameter of 20L was created around the fuselage of each helicopter. Another computational domain was created around the main rotor, as in Fig. 3b. 350,777 cells for the fuselage and 135,059 cells for the main rotor were generated by *MEGG3D*. Two sets were prepared to model two helicopters, where a set includes the domain for the fuselage and another domain for the main rotor.

While the validation test involves two computational domains for one helicopter model, the simulation in this section involves four domains because there are two helicopter models. Here, the fuselage domain of Helicopter 1 is defined as Domain 1F, the main rotor domain of Helicopter 1 as Domain 1R, the fuselage domain of Helicopter 2 as Domain 2F, and the main rotor domain of Helicopter 2 as Domain 2R. The variables are communicated between Domains 1F and 1R and between Domains 2F and 2R to model each helicopter. There is also communication between Domains 1F and 2F to represent the interaction of the flow fields that develop around each helicopter. This definition is illustrated in Fig. 6, where the domains for the fuselages are shown smaller and not to scale for the sake of simplicity.

Table 2 shows the initial conditions, where no flow or turbulence is assumed in the atmosphere in which the helicopters fly. The boundary conditions are the slip conditions at the object surfaces and the Riemann invariant boundary conditions at the outer boundaries of the fuselage grids. The conditions of the outer boundaries of the main rotor grids are the same as in Section 3.2. The helicopters engage in translational motion at a cruising speed of Mach 0.2 in the direction shown in Fig. 5 as modelled by the MCD method. The main rotors and the grids around them rotate counterclockwise at 395 rpm. The main rotors rotate only. While the actual helicopters lean slightly in the direction of their travel when they move forward, the simulations in this study do not model this.

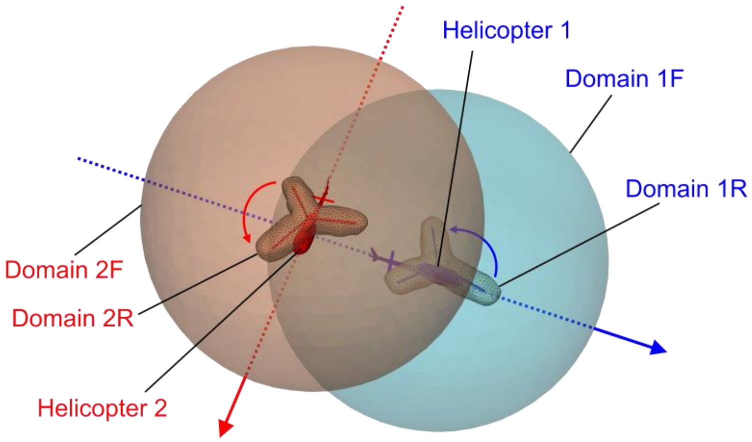

Fig. 6. Domain definitions used in the near-miss flight test cases

ICCS Camera Ready Version 2022
To cite this paper please use the final published version:
DOI: 10.1007/978-3-031-08760-8_28

Table 2. Initial conditions for the simulation of nearly missing helicopters

Whole region	
Density (ρ)	1.0
Flow velocity x component (u)	0.0
Flow velocity y component (v)	0.0
Flow velocity z component (w)	0.0
Pressure (p)	ρ/γ

4.3 Results and discussion

Case 1. Figures 7 and 8 illustrate the time histories of the aerodynamic coefficients and moment coefficients calculated for Helicopter 1, while figures 9 and 10 illustrate these calculated for Helicopter 2. The aerodynamic coefficients are computed with the following equations:

$$C_D = \frac{2F_D}{\rho V^2 S}, C_S = \frac{2F_S}{\rho V^2 S}, C_L = \frac{2F_L}{\rho V^2 S} \tag{3}$$

where C_D, C_S, C_L represent the drag coefficient, side-force coefficient, and lift coefficient, respectively. F_D, F_S, F_L indicate the drag, side force, and lift, respectively, which are the forces exerted on the helicopter in the x-, y-, and z-axes in Fig. 2, respectively. V denotes the characteristic speed, which in this study is the cruising speed of Mach 0.2. S is the characteristic area, which is represented by the main rotor disk area calculated using a main rotor radius of 5.35 m. The moment coefficients are computed with the following equations:

$$C_l = \frac{2M_l}{\rho V^2 SL}, C_m = \frac{2M_m}{\rho V^2 SL}, C_n = \frac{2M_n}{\rho V^2 SL} \tag{4}$$

where C_l, C_m, C_n represent the rolling moment coefficient, pitching moment coefficient, and yawing moment coefficient, respectively. M_l, M_m, M_n indicate the rolling moment, pitching moment, and yawing moment, respectively. L denotes the characteristic length, which is the fuselage length.

Figures 7 and 8 show that the aerodynamic coefficients and moment coefficients of Helicopter 1 do not change during the near miss. This suggests that Helicopter 1 is not affected by the flow that develops around Helicopter 2 because Helicopter 1 flies in front of Helicopter 2, where the flow field around Helicopter 2 does not develop.

On the other hand, Fig. 9 shows that the aerodynamic coefficients of Helicopter 2 are disturbed between 0.4 s and 0.8 s when it passes behind Helicopter 1. In particular, while the drag and side-force coefficients do not undergo a notable disturbance, the lift coefficient in Fig. 9 suggests that Helicopter 2 loses lift for approximately 0.3 s during the near miss. Figure 11 depicts the flow velocity z component distribution at 0.55 s in the xy-plane in the middle of the fuselage of the helicopters when the lift coefficient decreases noticeably. This indicates that Helicopter 2 flies into the area where the main

ICCS Camera Ready Version 2022
To cite this paper please use the final published version:
DOI: 10.1007/978-3-031-08760-8_28

rotor of Helicopter 1 generated a downward flow in the z direction. This flow field makes it difficult to create the ample pressure difference for obtaining the lift.

There is also a disturbance in the moment coefficients of Helicopter 2 in Fig. 10. The area through which Helicopter 2 passes during the near miss develops a complex flow field, with a spiral downward flow generated by the main rotor of Helicopter 1 as well as the flow that Helicopter 1's movement generates in the x direction. Helicopter 2 itself also creates its own flow with its movement and rotating main rotor. The interaction of their complex flow field affects the moment coefficients of Helicopter 2.

Case 2. Figures 12 and 13 illustrate the time histories of the aerodynamic coefficients and moment coefficients calculated for Helicopter 1 with Eq. (3), while figures 14 and 15 illustrate these calculated for Helicopter 2 with Eq. (4).

Analysing the graphs, we can see a disturbance in the moment coefficients of the two helicopters, but they do not experience a significant disturbance. However, a key point revealed by the graphs is that both helicopters lose their lift during the near miss. Moreover, the lifts decrease for approximately 0.4 s, which is longer than that of Helicopter 2 in Case 1. Figure 16 depicts the flow velocity z component distribution at 0.5 s in the xy-plane in the middle of the fuselage of Helicopter 2. This figure indicates that both helicopters are affected by the flow generated by each other during the near miss, which results in the decrease in the lift coefficient of not only Helicopter 2 but also Helicopter 1. In addition, the helicopters just fly in the complex flow field due to their trajectories. Since Helicopter 2 in Case 1 only passes perpendicularly through the complex flow field generated by Helicopter 1, the lift recovers faster than in Case 2.

5 Conclusions

This study computationally demonstrates two helicopters and examines the aerodynamic effect exerted on them during a near miss. The MGFV method is applied to the moving mesh to represent the motion of the helicopters. The long trajectories of the moving helicopters are successfully modelled by the MCD method. The flows generated by the rotating main rotors, as well as the flow interaction around the helicopters, are achieved by applying the overset approach, which allows the communication of the moving computational domains. In the validation test, the results computed by the in-house code are in agreement with those of *FaSTAR-Move*, confirming that the flow field variables are accurately interpolated between the overlapping grids in this study. In the near-miss flight test case where two helicopters pass each other perpendicularly, the lift of Helicopter 2, which flies behind Helicopter 1, decreases. On the other hand, in the case where Helicopter 2 passes horizontally underneath Helicopter 1, the lift decrease occurs for both helicopters. The disturbance is observed in the moment coefficients in both cases. These results show that the complex flow field around nearly missing helicopters is realised although this study uses a simplified model, indicating that this CFD approach is capable of simulating near-miss events involving aircraft. Future work will introduce the function of each component of aircraft and study the reaction to the flow field in a near miss as well as the suggested manoeuvring.

ICCS Camera Ready Version 2022
To cite this paper please use the final published version:
DOI: 10.1007/978-3-031-08760-8_28

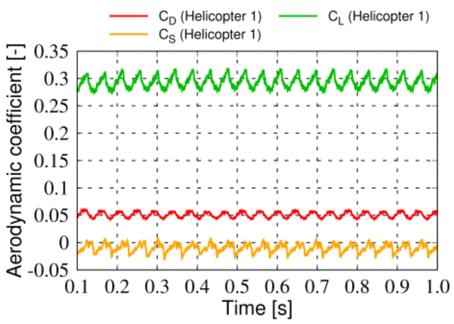

Fig. 7. Aerodynamic coefficient of Helicopter 1 (Case 1)

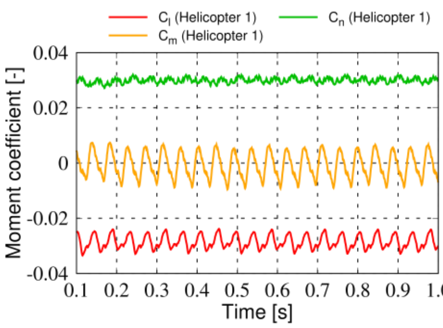

Fig. 8. Moment coefficient of Helicopter 1 (Case 1)

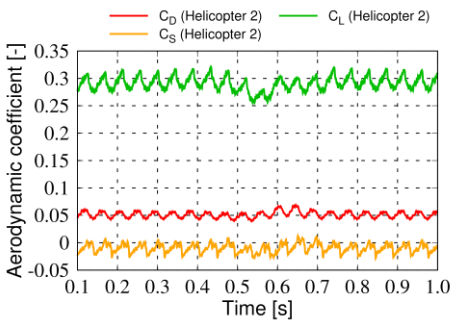

Fig. 9. Aerodynamic coefficient of Helicopter 2 (Case 1)

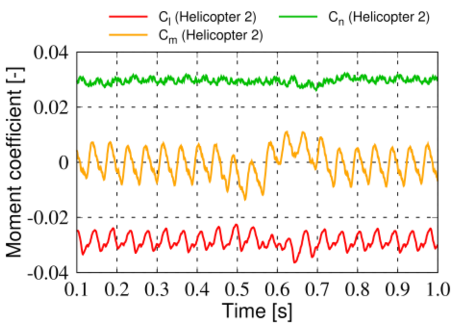

Fig. 10. Moment coefficient of Helicopter 2 (Case 1)

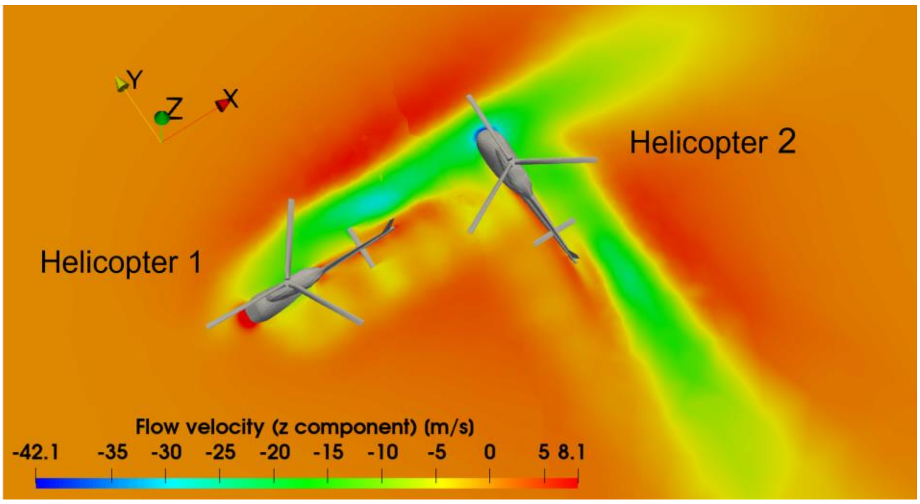

Fig. 11. Flow velocity z component distribution at 0.55 s (Case 1)

ICCS Camera Ready Version 2022
To cite this paper please use the final published version:
DOI: 10.1007/978-3-031-08760-8_28

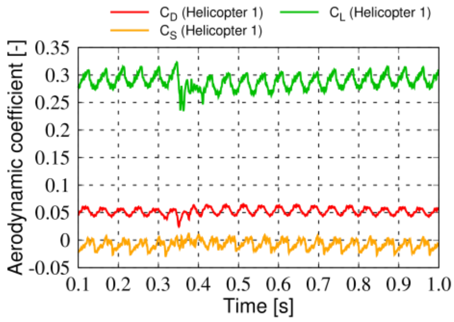

Fig. 12. Aerodynamic coefficient of Helicopter 1 (Case 2)

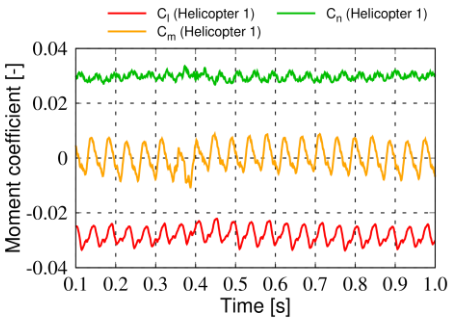

Fig. 13. Moment coefficient of Helicopter 1 (Case 2)

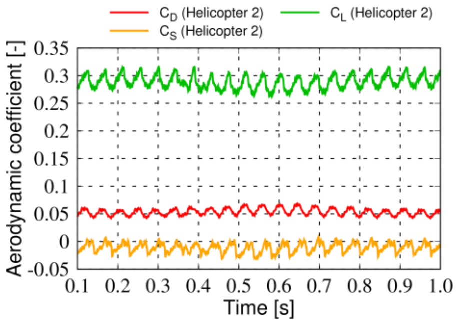

Fig. 14. Aerodynamic coefficient of Helicopter 2 (Case 2)

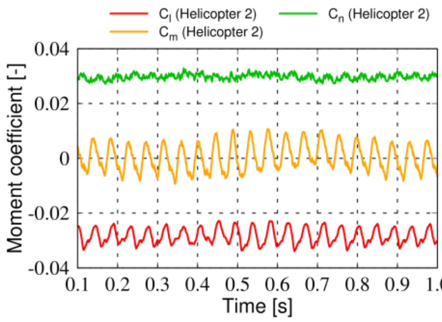

Fig. 15. Moment coefficient of Helicopter 2 (Case 2)

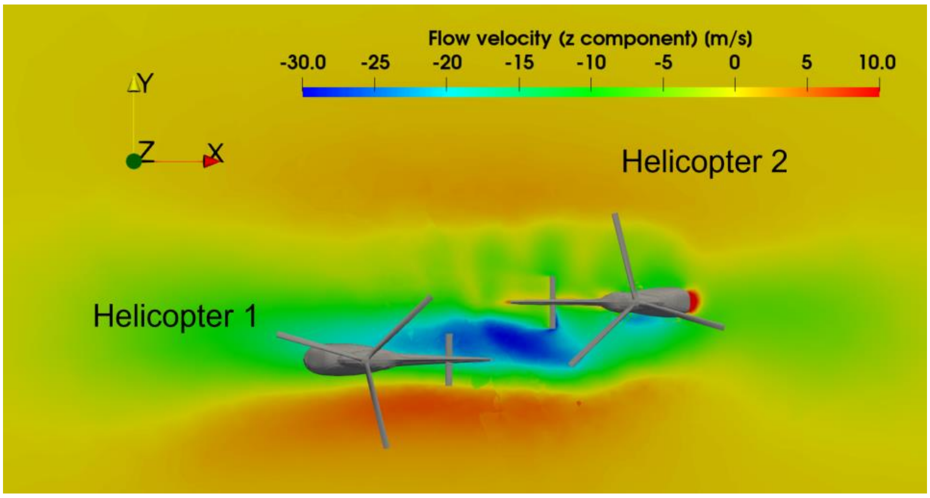

Fig. 16. Flow velocity z component distribution at 0.5 s (Case 2)

ICCS Camera Ready Version 2022
To cite this paper please use the final published version:
DOI: 10.1007/978-3-031-08760-8_28

Acknowledgements

This publication was subsidised by JKA through its promotion funds from KEIRIN RACE and by JSPS KAKENHI Grant Number 21K03856. A helicopter model from the VSP Hangar community (File ID# 359 [18]) was used in this study.

References

1. Australian Transport Safety Bureau, https://www.atsb.gov.au/publications/occurrence-briefs/2020/aviation/ab-2020-044/, last accessed 2022/02/18.
2. Biava, M. *et al.*: CFD prediction of air flow past a full helicopter configuration. Aerospace Science and Technology 19(1), 3–18 (2012).
3. Steijl, R. *et al.*: Sliding mesh algorithm for CFD analysis of helicopter rotor–fuselage aerodynamics. International Journal for Numerical Methods in Fluids 58(5), 527–549 (2008).
4. Crozon, C. *et al.*: Coupled flight dynamics and CFD—demonstration for helicopters in shipborne environment. The Aeronautical Journal 122(1247), 42–82 (2018).
5. Takii, A. *et al.*: Turning flight simulation of tilt-rotor plane with fluid-rigid body interaction. Journal of Thermal Science and Technology 15(2), JTST0021 (2020).
6. Matsuno, K.: Development and applications of a moving grid finite volume method. In: Topping, B. H. V. *et al.* (eds.) Developments and applications in engineering computational technology, Chapter 5, pp. 103–129. Saxe-Coburg Publications, Stirlingshire (2010).
7. Watanabe, K. *et al.*: Moving computational domain method and its application to flow around a high-speed car passing through a hairpin curve. Journal of Computational Science and Technology 3(2), 449–459 (2009).
8. Takii, A. *et al.*: Six degrees of freedom flight simulation of tilt-rotor aircraft with nacelle conversion. Journal of Computational Science 44, 101164 (2020).
9. Yamakawa, M. *et al.*: Optimization of knee joint maximum angle on dolphin kick. Physics of Fluids 32(6), 067105 (2020).
10. Nishimura, M. *et al.*: Moving computational multi-domain method for modelling the flow interaction of multiple moving objects. Advances in Aerodynamics 4(1), 5 (2022).
11. Roe, P. L.: Approximate Riemann solvers, parameter vectors, and difference schemes. Journal of Computational Physics 43(2), 357–372 (1981).
12. Hishida, M. *et al.*: A new slope limiter for fast unstructured CFD solver FaSTAR (*in Japanese*). In: JAXA Special Publication: Proceedings of 42nd Fluid Dynamics Conference / Aerospace Numerical Simulation Symposium 2010, JAXA-SP-10-012 (2011).
13. Nakahashi, K. *et al.*: Intergrid-boundary definition method for overset unstructured grid approach. AIAA Journal 38(11), 2077–2084 (2000).
14. Hashimoto, A. *et al.*: Toward the Fastest Unstructured CFD Code “FaSTAR”. 50th AIAA Aerospace Sciences Meeting including the New Horizons Forum and Aerospace Exposition 2012, AIAA 2012-1075 (2012).
15. Taniguchi, S. *et al.*: Numerical Analysis of Propeller Mounting Position Effects on Aerodynamic Propeller/Wing Interaction. AIAA SCITECH 2022 forum (2022).
16. Ito, Y.: Challenges in unstructured mesh generation for practical and efficient computational fluid dynamics simulations. Computers & Fluids 85, 47–52 (2013).
17. Shima, E. *et al.*: Parameter-Free Simple Low-Dissipation AUSM-Family Scheme for All Speeds. AIAA Journal 49(8), 1693–1709 (2011).
18. VSP Hangar, http://hangar.openvsp.org/vspfiles/359, last accessed 2022/02/18.

DOI: 10.1007/978-3-031-08760-8_28